IEEE Access
Multidisciplinary | Rapid Review | Open Access Journal

Received August 16, 2019, accepted September 22, 2019, date of publication September 26, 2019, date of current version October 21, 2019.

Digital Object Identifier 10.1109/ACCESS.2019.2943915

A Flatness-Based Nonlinear Control Scheme for Wire Tension Control of Hoisting Systems

WANSHUN ZANG[1,2], GANG SHEN[1,2], GUANGCHAO RUI[3,4], XIANG LI[1,2], GE LI[1,2], AND YU TANG[1,2]

[1]School of Mechatronic Engineering, China University of Mining and Technology, Xuzhou 221116, China
[2]Jiangsu Key Laboratory of Mine Mechanical and Electrical Equipment, China University of Mining and Technology, Xuzhou 221116, China
[3]Seventh Thirteen Institute of China Shipbuilding Industry Corporation, Zhengzhou 450000, China
[4]Key Laboratory of Underwater Intelligent Equipment in Henan Province, Zhengzhou 450000, China

Corresponding author: Gang Shen (shenganghit@163.com)

This work was supported by the Future Scientists Program of "Double First Class" of the China University of Mining and Technology under Grant 2019WLKXJ034.

ABSTRACT A double-rope winding hoisting system (DRWHS) is usually employed to transport weight or workers in mines usually from ultra-deep underground (>1000m). An electro-hydraulic servo system (EHSS), which consists of two hydraulic cylinders, two movable headgear sheaves and lots of indispensable sensors, is employed to actively coordinate two wire tensions. The nonlinear dynamic model of the DRWHS is introduced and it is divided into two subsystems, i.e., the hoisting system and the EHSS with state space representations. However, as a complex machine-electricity-hydraulic system, the accurate dynamic model of the DRWHS is usually hard to obtain. Therefore, a flatness-based controller (FBC), which is insensitive to unmodeled characteristics of the dynamic model and measurement noises of sensors, is proposed to improve the tension coordination of two wire tensions of the DRWHS. The explicit FBC design schemes for the DRWHS and the control law are presented, and the stability of the proposed controller are proved by defining a Lyapunov function. The controller proposed is characterized by no derivatives of state variables and lower controller design complication so that measurement noises of sensors and unmodeled characteristics are not amplified. An experimental bench of the DRWHS is established to verify the performance of the proposed controller. Experimental results show that the proposed controller exhibits a better performance on the tension coordination control of two wire ropes compared with a backstepping controller (BC) and a conventional proportional-integral (PI) controller.

INDEX TERMS Double-rope winding hoisting system, flatness-based control, wire tension control.

NOMENCLATURE

$l_{ri}(i = 1, 2)$	rotation lengths of two winding drums
$l_{ci}(i = 1, 2)$	lengths of two catenaries in the process of hoisting or lowering the conveyance
$l_{hi}(i = 1, 2)$	lengths of two vertical hoisting wire ropes in the process of hoisting or lowering the conveyance;
$u_i(i = 1, 2)$	displacements of two movable headgear sheaves
$\varphi_i(i = 1, 2)$	angle between two catenaries and the horizontal plane
$a_i(i = 1, 2)$	horizontal distance between junctions of two wire ropes and the conveyance
and the	barycenter of the conveyance
$b_i(i = 1, 2)$	longitudinal distance between top and bottom surfaces of the conveyance and the barycenter of the conveyance
$k_{si}(i = 1, 2, 3, 4)$	lateral equivalent stiffness of four pairs of the spring-damper model
$c_{si}(i = 1, 2, 3, 4)$	lateral equivalent damping coefficient of four pairs of the spring-damper model
l_{h10}, l_{h20}	the initial lengths of two vertical hoisting wire ropes
x_c	the vertical displacement of the conveyance barycenter

The associate editor coordinating the review of this manuscript and approving it for publication was Huanqing Wang.

y_c	the lateral displacement of the conveyance barycenter
θ	the counterclockwise rotation angle of the conveyance
r_1	the radius of the left movable headgear sheave
r_2	the radius of the right movable headgear sheave
τ_1	the tension of the left wire rope
τ_2	the tension of the right wire rope
k_{h1}	the stiffness of the left vertical hoisting rope
k_{h2}	the stiffness of the right vertical hoisting rope
c_{h1}	the damping coefficients of the left vertical hoisting rope
c_{h2}	the damping coefficients of the right vertical hoisting rope
k_{c1}	the stiffness of the left catenary rope
k_{c2}	the stiffness of the right catenary rope
c_{c1}	the damping coefficients of the left catenary rope
c_{c2}	the damping coefficients of the right catenary rope
L	the acceleration of gravity
n_R	the number of the rope guides
T_L	the rope guide tension
L	the overall length of the rope guides
L_1	the rope guide length between the top of conveyance and the top anchor point
L_2	the rope guide length between the bottom of conveyance and the bottom anchor point
T_H	the hoisting rope tension
n_H	the number of the hoisting ropes for a single conveyance
ρ	the unit mass of wire rope
M	the mass matrix of the DRWHS
C	the damping matrix of the DRWHS
K	the stiffness matrix of the DRWHS
F	the non-potential force vector of the DRWHS
Q_L	the load flow from the valve to the actuator chambers
A_p	the effective area of chamber
x_p	the piston rod displacement
V_t	the total volume
β_e	the effective bulk modulus
C_{tl}	the total leakage coefficient
x_v	the displacement of the servo valve spool
C_d	the discharge coefficient of the servo valve
w	the area gradient of the servo valve spool
ρ_o	the density of oil
P_s	the pressure of supply oil
P_L	the load pressure
F_g	the load force of the hydraulic cylinder
k_v	the proportional coefficient
u_L	the control voltage of the servo valve
$u_{\max}$	the maximum control voltage of the servo valve
Q_{r}	the rated flow of the servo valve
ΔP_{r}	the rated pressure drop of the servo valve

I. INTRODUCTION

A mine hoisting system, which is usually utilized to transport weight or workers from underground, is the throat of a mine. At present, there are mainly two types mine hoisting systems employed in mines, i.e., multi-rope friction hoisting systems and single rope winding hoisting systems. With the decrease of shallow (500-800m) and deep (800-1000m) mineral resources, it has become a trend to explore ultra-deep (>1000m) mineral resources [1]. Multi-rope friction hoisting systems and single rope winding hoisting systems have both already been proved to have significant limitations when being utilized for ultra-deep coal mines [1]–[3]. In order to realize ultra-deep hoisting, Blair multi-rope hoisting systems have been utilized in South Africa [4]. In this paper, based on Blair multi-rope hoisting systems, a double-rope winding hoisting system (DRWHS) is presented in FIGURE 1. As shown in FIGURE 1, a twin winding drum is utilized to drive two wire ropes, which will hoist or lower two conveyances. The twin winding drum is wound with one hoisting wire rope respectively in the opposite direction, which indicates that when one of two conveyances is being hoisted, the other is being lowered. Two hydraulic cylinders are employed to actively coordinate tensions of two wire ropes.

However, when the DRWHS is in operation, some factors like different manufacturing precisions between the twin winding drum, the asynchrony winding of two wire ropes, difference length between two wire ropes, different depths of winding grooves and difference of elastic modulus of two wire ropes, will result in different end displacements of two wire ropes, which will further result in the tension difference between two wire ropes. What's more, when the tension difference reaches to the weight of the conveyance being mainly supported by one wire rope, then the tensile stress of the wire rope will be too big to make the rope be broken accidentally. As the throat of a coal mine, the hoisting system's safety operation relates directly to the mining efficiency and workers' safety. Therefore, it is fatally important to adjust the tension difference to make the weight of the conveyance evenly distribute on two wire ropes, which will extend the using life of wire ropes. Nowadays, a device, which consists of two suspended hydraulic cylinders and a communicating vessel, has been widely utilized to coordinate the tension difference passively [5]. When tensions of two wire ropes are different, the oil in one hydraulic cylinder will be squeezed into the other one, which will decrease the tension difference of two wire ropes. However, this device can't actively and quickly adjust the tension difference, which won't be suitable for the DRWHS with heavy conveyances at a high velocity. Therefore, an active coordination device, which consists of two movable headgear sheaves, two active hydraulic cylinders, a hydraulic pump station and some dispensable sensors and mechanical structures, is presented to actively and quickly coordinate tensions of two wire ropes. Therefore, tensions of two wire ropes can be actively adjusted

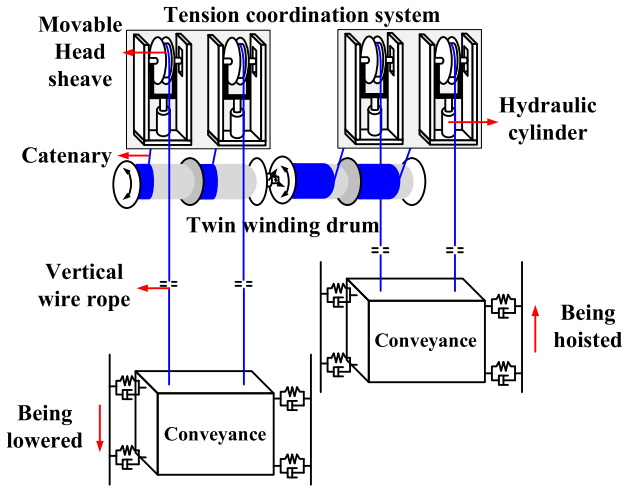

FIGURE 1. The DRWHS.

by two active hydraulic cylinders pushing and pulling two moveable headgear sheaves.

A conventional proportional-integral (PI) controller can no doubt coordinate two tensions of two wire ropes [6], [7]. However, the performance of the PI controller need to be improved. When the nonlinear model of a system is established, controllers like sliding mode controllers [1], [8], [9], robust controllers [10]–[12], adaptive controllers [13]–[16] can be designed. These controllers above all improve the coordination of two tensions of two wire ropes. Especially, controllers via the backstepping approach is really powerful [17]–[22] and exhibits better performances than these above controllers. However, when controllers via the backstepping approach is applied to a n-order system ($n \geq 3$), the need for repeated derivations of virtual controls in each step of controllers' design may result in a large amount of computation and computational expansion. And repeated derivations of virtual controls will definitely need repeated derivations of state variables of a system, which will amplify measurement noises of sensors and unmodeled characteristics, and decrease the tracking accuracy. Therefore, some scholars have pursued methods to simplify controllers via the backstepping approach. In order to avoid repeated derivations of virtual controls in each step of controllers' design, command filtered backstepping controllers are proposed [23]–[25]. Command filter is a prefilter with a state space representation, whose characteristic equation is selected to be stable and to specify the desired bandwidth and the transient response. Therefore, derivatives of virtual controls in the backstepping approach can be obtained directly through the command filter designed, which avoids repeated derivatives of virtual controls in the backstepping approach. Flatness is an inherit property of a nonlinear system and it can be obtained by a series of algebraic operations [26]. Flatness based controllers (FBCs) can be designed if outputs of a system have the same dimension as inputs and, inputs of the system and system states can be expressed in terms of outputs of the system and finite numbers of their time derivatives. Nowadays, FBCs have been widely applied in many nonlinear systems to simplify their control laws and improve their performances, such as helicopter systems [27], hovercraft systems [28], chemical reactor systems [29], inverter systems [30], piezoelectric actuator systems [31], three-axis platform systems [32] and so on. The FBC for the electro-hydraulic servo system (EHSS) are proposed in references [33]–[35], and its flatness property are analyzed. Subsequently, based on the concept of flatness, FBCs are employed for the servo-valve system [36]and the torque tracking control of the electro-hydraulic loading system [37], [38] to improve their performances.

An accurate system model is always essential to design advanced nonlinear controllers [39]. However, the DRWHS is a typical complex machine-electricity-hydraulic system: 1) When the DRWHS is in operations, complex mechanical structures including a mechanical support system, two hydraulic cylinders, two hydraulic winches, two wire ropes and two moveable head sheaves will definitely engender structural vibrations, which are usually hard to model; 2) The complex throttling characteristics and hydraulic fluid compressibility brings significant nonlinear dynamics and make the accurate dynamic model of the EHSS hard to establish. What' more, parameters like the effective bulk modulus and the total leakage coefficient are usually hard to determine, which will bring parameter uncertainties; 3) There are lots of sensors including an angle sensor, four pressure transmissions, two displacement sensors employed to support operations of nonlinear controllers for the DRWHS. Sensors inevitably have measurement noises, which will decrease the tension coordination. What's more, in a practical modern mine, the DRWHS always operates with heavy conveyances at a high velocity. Therefore, the repeated derivation of virtual control in each step of controllers' design will definitely amplify measurement noises of sensors and unmodeled characteristics of the DRWHS, which will decrease the tension coordination. In order to simplify controllers' design and improve the tension coordination, a FBC, which is insensitive to unmodeled characteristics and measurement noises of sensors, is proposed to improve the tension coordination of two wire ropes in the DRWHS.

The main contribution of the paper is to present an easy to design and efficient FBC for the complex machine-electricity-hydraulic DRWHS to improve the tension coordination of two wire ropes and its verification on the experimental bench of the DRWHS. The proposed FBC is characterized by no derivatives of the state variables and lower controller design complication so that measurement noises and unmodeled characteristics are not amplified. The stability of the overall closed-loop is proven based on a Lyapunov function. In order to verify the performance of the proposed controller, a series of comparative experimental studies are conducted on the experimental bench. The experimental results verify the efficiency of the proposed controller is better than a backstepping controller (BC) and a PI controller.

This paper is organized as follows. In section 2, the dynamic of the DRWHS is presented. Section 3 shows the controller design for the hoisting system and the electro-hydraulic servo system. The experimental setup and the main results are shown in section 4. The conclusion is summarized in section 5.

II. DYNAMIC MODEL OF THE DRWHS

Fig. 2 shows the schematic of the DRWHS, which can be shown that it can be divided into two parts: a hoisting system and an EHSS.

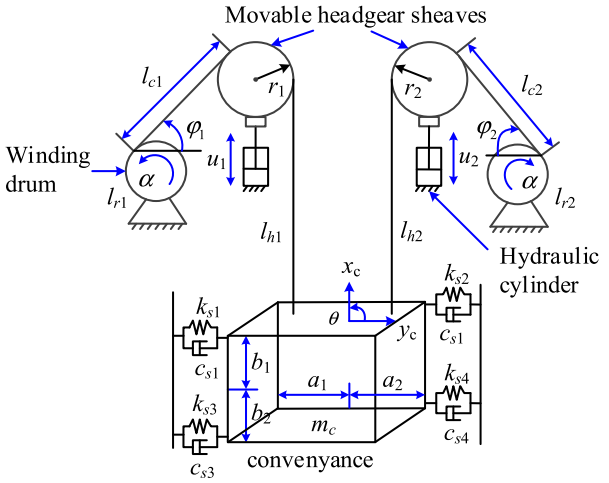

FIGURE 2. Schematic of the DRWHS.

A. DYNAMIC MODEL OF THE HOISTING SYSTEM

Consider the upward movement as the positive direction, lengths of two vertical hoisting wire ropes in the process of hoisting or lowering the conveyance can be expressed as follows:

$$l_{h1} = l_{h10} - l_{r1} - u_1 \sin(\varphi_1) \tag{1}$$

$$l_{h2} = l_{h20} - l_{r2} - u_2 \sin(\varphi_2) \tag{2}$$

Stiffness of a flexible shaft guide is time varying, which can be represented as [40]

$$k = n_R \frac{T_L L}{L_1 L_2} + n_H \frac{T_H}{L_1} \tag{3}$$

Then, tensions of two wire ropes can be expressed as follows:

$$\begin{cases} \tau_1 + \tau_2 = m_c(g + \ddot{x}_c) \\ -\tau_1(a_1 + b_1\theta) + \tau_2(a_2 - b_1\theta) = 0 \end{cases} \tag{4}$$

Therefore, from Eq. (4), when the counterclockwise rotation angle of the conveyance $\theta = 0$, two tensions of two wire ropes are equal, namely, the tension difference is equal to zero.

According to references [1] and [17], the dynamic model of the DRWHS can be expressed as

$$M\ddot{q} + C\dot{q} + Kq = F. \tag{5}$$

where $\ddot{q}$, $\dot{q}$ and q are the generalized acceleration, velocity and displacement, respectively. M, C, K and F are the mass matrix, the damping matrix, the stiffness matrix, and the non-potential force vector of the DRWHS, respectively, which are expressed in (6)–(9), as shown at the bottom of this page. With $a_1 = a_2$, $b_1 = b_2$ and $u_1 = u = -u_2$, Eq. (5) can be simplified as

$$A\ddot{\theta} + B\dot{\theta} + C\theta = Q\ddot{u} + W\dot{u} + Ru + F_0. \tag{10}$$

where

$$\begin{cases} A = M_{33} \\ B = C_{33} \\ C = K_{33} \\ Q_e = \frac{1}{6}\rho l_{h1} a_1 (1 + \sin(\varphi_1)) + \frac{1}{6}\rho l_{h2} a_2 (1 + \sin(\varphi_2)) \\ W = (-\frac{1}{6}\rho \dot{l}_{h1} + c_{h1}) a_1 (1 + \sin(\varphi_1)) \\ \quad + (-\frac{1}{6}\rho \dot{l}_{h2} + c_{h2}) a_1 (1 + \sin(\varphi_2)) \\ R = k_{h1} a_1 (1 + \sin(\varphi_1)) + k_{h2} a_2 (1 + \sin(\varphi_2)) \\ F_0 = \frac{1}{6}\rho l_{h1} a_1 \ddot{l}_{r1} - \frac{1}{6}\rho l_{h2} a_2 \ddot{l}_{r2} + (-\frac{1}{6}\rho \dot{l}_{h1} + c_{h1}) a_1 \dot{l}_{r1} \\ \quad -(-\frac{1}{6}\rho \dot{l}_{h2} + c_{h2}) a_2 \dot{l}_{r2} + k_{h1} a_1 l_{r1} - k_{h2} a_2 l_{r2} - M_{31}\ddot{x}_c \\ \quad -C_{31}\dot{x}_c - K_{31} x_c + \frac{1}{2}\rho g l_{h1} a_1 - \frac{1}{2}\rho g l_{h2} a_2. \end{cases} \tag{11}$$

$$M = \begin{bmatrix} m_c + \frac{1}{3}\rho l_{h1} + \frac{1}{3}\rho l_{h2} & 0 & -\frac{1}{3}\rho l_{h1} a_1 + \frac{1}{3}\rho l_{h2} a_2 \\ 0 & m_c & 0 \\ -\frac{1}{3}\rho l_{h1} a_1 + \frac{1}{3}\rho l_{h2} a_2 & 0 & I_c - \frac{1}{3}\rho l_{h1} a_1^2 + \frac{1}{3}\rho l_{h2} a_2^2 \end{bmatrix} \tag{6}$$

$$C = \begin{bmatrix} c_{h1} + \frac{1}{3}\rho \dot{l}_{h1} + c_{h2} + \frac{1}{3}\rho \dot{l}_{h2} & 0 & -\left(c_{h1} + \frac{1}{3}\rho \dot{l}_{h1}\right) a_1 + \left(c_{h2} + \frac{1}{3}\rho \dot{l}_{h2}\right) a_2 \\ 0 & c_{s1} + c_{s2} + c_{s3} + c_{s4} & -c_{s1} b_1 + c_{s2} b_2 - c_{s3} b_1 + c_{s4} b_2 \\ -\left(c_{h1} + \frac{1}{3}\rho \dot{l}_{h1}\right) a_1 + \left(c_{h2} + \frac{1}{3}\rho \dot{l}_{h2}\right) a_2 & -c_{s1} b_1 + c_{s2} b_2 - c_{s3} b_1 + c_{s4} b_2 & \left(c_{h1} + \frac{1}{3}\rho \dot{l}_{h1}\right) a_1^2 + \left(c_{h2} + \frac{1}{3}\rho \dot{l}_{h2}\right) a_2^2 + b_1^2 c_{s1} + b_2^2 c_{s2} + b_1^2 c_{s3} + b_2^2 c_{s4} \end{bmatrix} \tag{7}$$

$$K = \begin{bmatrix} k_{h1} + k_{h2} & 0 & -k_{h1} a_1 + k_{h2} a_2 \\ 0 & k_{s1} + k_{s2} + k_{s3} + k_{s4} & -k_{s1} b_1 + k_{s2} b_2 - k_{s3} b_1 + k_{s4} b_2 \\ -k_{h1} a_1 + k_{h2} a_2 & -k_{s1} b_1 + k_{s2} b_2 - k_{s3} b_1 + k_{s4} b_2 & k_{h1} a_1^2 + k_{h2} a_2^2 + b_1^2 k_{s1} + b_2^2 k_{s2} + b_1^2 k_{s3} + b_2^2 k_{s4} \end{bmatrix} \tag{8}$$

$$F = \begin{bmatrix} -\frac{1}{6}\rho l_{h1} \left[\ddot{l}_{r1} + \ddot{u}_1(1 + \sin\varphi_1)\right] - \frac{1}{6}\rho l_{h2} \left[\ddot{l}_{r2} + \ddot{u}_2(1 + \sin\varphi_2)\right] + \left(-\frac{1}{6}\rho \dot{l}_{h1} + c_{h1}\right) \left[\dot{l}_{r1} + \dot{u}_1(1 + \sin\varphi_1)\right] \\ + \left(-\frac{1}{6}\rho \dot{l}_{h2} + c_{h2}\right) \left[\dot{l}_{r2} + \dot{u}_2(1 + \sin\varphi_2)\right] + k_{h1} \left[l_{r1} + u_1(1 + \sin\varphi_1)\right] + k_{h2} \left[l_{r2} + u_2(1 + \sin\varphi_2)\right] - m_c g - \frac{1}{2}\rho g l_{h1} - \frac{1}{2}\rho g l_{h2} \\ 0 \\ \frac{1}{6}\rho l_{h1} a_1 \left[\ddot{l}_{r1} + \ddot{u}_1(1 + \sin\varphi_1)\right] - \frac{1}{6}\rho l_{h2} a_2 \left[\ddot{l}_{r2} + \ddot{u}_2(1 + \sin\varphi_2)\right] + \left(-\frac{1}{6}\rho \dot{l}_{h1} + c_{h1}\right) a_1 \left[\dot{l}_{r1} + \dot{u}_1(1 + \sin\varphi_1)\right] \\ -\left(-\frac{1}{6}\rho \dot{l}_{h2} + c_{h2}\right) a_2 \left[\dot{l}_{r2} + \dot{u}_2(1 + \sin\varphi_2)\right] + k_{h1} a_1 \left[l_{r1} + u_1(1 + \sin\varphi_1)\right] - k_{h2} a_2 \left[l_{r2} + u_2(1 + \sin\varphi_2)\right] + \frac{1}{2}\rho g l_{h1} a_1 - \frac{1}{2}\rho g l_{h2} a_2 \end{bmatrix} \tag{9}$$

Values of k_{h1} and k_{h2} are much larger than those of c_{h1} and c_{h2} so that Eq. (10) can be further simplified as

$$A\ddot{\theta} + B\dot{\theta} + C\theta = Ru + F_0. \tag{12}$$

B. DYNAMIC MODEL OF THE EHSS

The control input u shown in Eq. (12) is obtained from the EHSS. FIGURE 3 presents the electro-hydraulic cylinder configuration. The dynamic model of the EHSS is shown as follows. By employing the flow continuity equation, the load flow Q_{L} from the valve to actuator chambers can be formulated as

$$A_p\dot{x}_p + C_{tl}P_L + \frac{V_t}{4\beta_e}\dot{P}_L = Q_L. \tag{13}$$

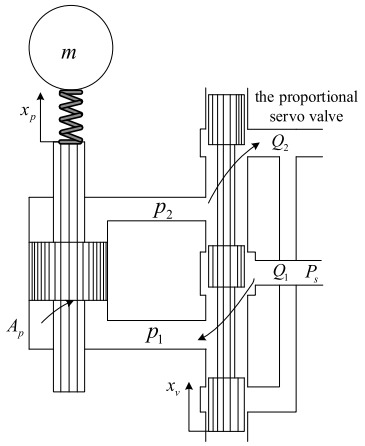

FIGURE 3. Electro-hydraulic cylinder configuration.

The force balance equation for the hydraulic cylinder yields

$$-m\ddot{x}_p - B_p\dot{x}_p + A_pP_L = F_g. \tag{14}$$

The load flow of a hydraulic cylinder is controlled by the displacement of a servo valve's spool. Therefore,

$$Q_L = C_d \mathrm{w} x_v \sqrt{\frac{P_s - sgn(x_v)P_L}{\rho_o}}. \tag{15}$$

Because the response speed of the servo valve is much higher than the hydraulic system, the dynamic of the servo valve can be ignored. Therefore, the simplified model of the servo valve yields

$$x_v = k_v u_L \tag{16}$$

From Eqs. (15) and (16), the load flow of the hydraulic cylinder can be rewritten as

$$Q_L = C_d \mathrm{w} k_v u_L \sqrt{\frac{P_s - sgn(u_L)P_L}{\rho_o}}. \tag{17}$$

Actually, C_d and w are both estimated values, therefore, it is really a hard work to obtain the control voltage of the servo valve directly. However, the rated flow rate of the servo valve at the rated pressure drop is always easy to obtain.

$$Q_r = C_d \mathrm{w} k_v u_{\max} \sqrt{\frac{\Delta P_r}{\rho_o}} \tag{18}$$

From Eqs. (17) and (18),

$$\frac{Q_L}{Q_r} = \frac{C_d \mathrm{w} k_v u_L \sqrt{\frac{P_s - sgn(u_L)P_L}{\rho_o}}}{C_d \mathrm{w} k_v u_{\max} \sqrt{\frac{\Delta P_r}{\rho_o}}} = \frac{u_L\sqrt{P_s - sgn(u_L)P_L}}{u_{\max}\sqrt{\Delta P_r}}. \tag{19}$$

Therefore, the control voltage of the servo valve yields

$$u_L = \frac{Q_L}{Q_r\sqrt{\frac{P_s - sgn(u_L)P_L}{\Delta P_r}}} u_{\max}. \tag{20}$$

C_d, w and k_v are all positive, therefore, from Eq. (17),

$$\begin{aligned} sgn(Q_L) &= sgn\left(C_d \mathrm{w} k_v u_L \sqrt{\frac{P_s - sgn(u_L)P_L}{\rho_o}}\right) \\ &= sgn(u_L). \end{aligned} \tag{21}$$

From all above, the control input of the servo valve yields

$$u_L = \frac{Q_L}{Q_r}\sqrt{\frac{\Delta P_r}{P_s - sgn(Q_L)P_L}} u_{\max}. \tag{22}$$

C. DYNAMIC MODEL OF THE DRWHS

State variables can be defined by $x = [x_1, x_2, x_3, x_4, x_5]^T = [\theta, \dot{\theta}, x_p, \dot{x}_p, P_L]^T$, and the DRWHS can be presented in a state space form as

$$\begin{cases} \dot{x}_1 = x_2 \\ \dot{x}_2 = -h_1x_2 - h_2x_1 + h_3x_3 + f \\ \dot{x}_3 = x_4 \\ \dot{x}_4 = a_1x_5 - a_2x_4 - a_3F_g \\ \dot{x}_5 = -a_4x_4 - a_5x_5 + a_6Q_L. \end{cases} \tag{23}$$

where $h_1 = B/A$, $h_2 = C/A$, $h_3 = R/A$, $f = F_0/A$, $a_1 = A_p/m$, $a_2 = B_p/m$, $a_3 = 1/m$, $a_4 = 4\beta_eA_p/V_t$, $a_5 = 4\beta_eC_{tl}/V_t$, and $a_6 = 4\beta_e/V_t$.

By referring to Eq. (23), it can be seen that the time derivative of the state variable x_3 is not related to x_2; therefore, Eq. (23) can be divided as two parts, where the state variable x_3 can be regarded as the control input of part one and reference signal of part two. In this case, state variables can be defined by $x_1 = [x_1, x_2]^T = [\theta, \dot{\theta}]^T$, $x_2 = [x_3, x_4, x_5]^T = [x_p, \dot{x}_p, P_L]^T$, and the entire system can be presented in the following state space forms:

$$\begin{cases} \dot{x}_1 = x_2 \\ \dot{x}_2 = -h_1x_2 - h_2x_1 + h_3x_3 + f \end{cases} \tag{24}$$

$$y_1 = x_1$$

$$\begin{cases} \dot{x}_3 = x_4 \\ \dot{x}_4 = a_1x_5 - a_2x_4 - a_3F_g \\ \dot{x}_5 = -a_4x_4 - a_5x_5 + a_6Q_L \end{cases} \tag{25}$$

$$y_2 = x_3$$

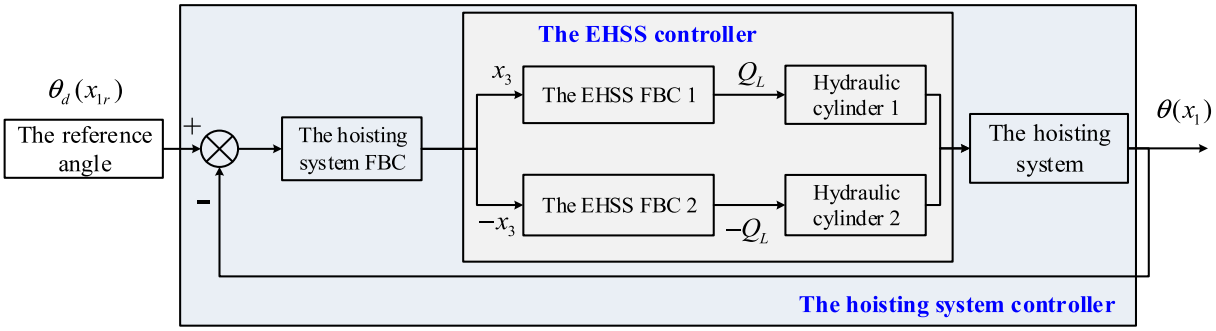

FIGURE 4. The schematic of the closed-loop control system.

Assumption: For the hoisting system, θ and $\dot{\theta}$ are both bounded. For the EHSS, the desired displacement x_p, its velocity $\dot{x}_p$, acceleration $\ddot{x}_p$, and x_p are all bounded.

III. CONTROLLER DESIGN

In this section, we mainly design FBCs for the hoisting system and the EHSS according to the concept of flatness. FIGURE 4 presents the schematic of the closed-loop control system. When the conveyance is being hoisted or lowered, once the counterclockwise rotation angle of the conveyance is not equal to zero, the hoisting system FBC will solve out displacements of two hydraulic cylinders according to the dynamic of the DRWHS. Then the EHSS FBC 1 and 2 will drive two hydraulic cylinders to actively push or pull two movable headgear sheaves. Then the counterclockwise rotation angle will be actively adjusted to zero.

A. FLATNESS PROPERTY IN NONLINEAR SYSTEMS

Consider the following nonlinear system [29][35]

$$\dot{x} = f(x, u). \tag{26}$$

where x denotes the system state and u denotes the control input with the same dimension as the system output y. And it is assumed that the vector function f is smooth. If the system output y can be expressed in terms of the system state x, the control input u and finite numbers of its time derivatives, which is shown as follow.

$$y = \chi(x, \dot{u}, \ddot{u}, \ldots, u^{(p)}). \tag{27}$$

Furtherly, the system state x and the system input u can be expressed in terms of y and a finite number of its time derivatives.

$$x = \chi(y, \dot{y}, \ddot{y}, \ldots, y^{(q)}). \tag{28}$$
$$u = \gamma(y, \dot{y}, \ddot{y}, \ldots, y^{(q+1)}). \tag{29}$$

Then (26) is called flat and the system output y is called the flat output. The flatness property allows us to explicitly analyze the system model by formally calculating the system variables as functions of the flat output and its derivatives according to (28) and (29).

B. FBC FOR THE HOISTING SYSTEM

According to the FBC design method, in the hoisting system (24), the output is $y_1 = x_1$ and the control input is $u_h = x_3$. Therefore, for the hoisting system (24), we can obtain flatness functions from $y_1, \dot{y}_1, \ddot{y}_1$ to $\boldsymbol{x}_1$ and the control input u_h as

$$\begin{bmatrix} x_1 \\ x_2 \\ u_h \end{bmatrix} = \begin{bmatrix} y_1 \\ \dot{y}_1 \\ (h_1\dot{y}_1 + h_2 y_1 - f + \ddot{y}_1)/h_3 \end{bmatrix}. \tag{30}$$

If we define the desired state $\boldsymbol{x}_{1d} = [x_{1d}, x_{2d}]^T = [y_{1d}, \dot{y}_{1d}]^T$, where y_{1d} denotes the desired output, namely, the reference signal. Therefore, the dynamics of the desired state $\boldsymbol{x}_{1d} = [x_{1d}, x_{2d}]^T$ is

$$\frac{d}{dt}\begin{bmatrix} x_{1d} \\ x_{2d} \end{bmatrix} = \begin{bmatrix} x_{2d} \\ -h_1 x_{2d} - h_2 x_{1d} + h_3 u_{hd} + f \end{bmatrix}. \tag{31}$$

Therefore, we can obtain the open-loop control input u_{hd} as

$$u_{hd} = (h_1\dot{y}_{1d} + h_2 y_{1d} - f + \ddot{y}_{1d})/h_3 \tag{32}$$

Let the tracking error be $\boldsymbol{z}_1 = [z_1, z_2]^T = [x_{1d} - x_1, x_{2d} - x_2]^T$. Therefore, the tracking error dynamics yield

$$\begin{bmatrix} \dot{z}_1 \\ \dot{z}_2 \end{bmatrix} = \begin{bmatrix} z_2 \\ -h_1 z_2 - h_2 z_1 - h_3(u_{hd} - u_h) \end{bmatrix}. \tag{33}$$

with $u_{hd} = u_h$, we can obtain

$$\begin{bmatrix} \dot{z}_1 \\ \dot{z}_2 \end{bmatrix} = \begin{bmatrix} z_2 \\ -h_1 z_2 - h_2 z_1 \end{bmatrix}. \tag{34}$$

In matrix form,

$$\dot{\boldsymbol{z}}_1 = \boldsymbol{A}_h \boldsymbol{z}_1. \tag{35}$$

where, $\boldsymbol{A}_h = \begin{bmatrix} 0 & 1 \\ -h_2 & -h_1 \end{bmatrix}$.

Obviously, $\boldsymbol{A}_h$ is Hurwitz. Thus $\boldsymbol{z}_1$ converges to zero. However, the convergence speed cannot be arbitrarily chosen by the open-loop controller. Therefore, we design the control input u_h with state feedbacks as

$$u_h = u_{hd} + \frac{1}{h_3}\boldsymbol{K}_1 \boldsymbol{z}_1 \tag{36}$$

where $\boldsymbol{K}_1 = [k_1, k_2]$. Therefore, the tracking error dynamics with state feedbacks yield

$$\dot{z}_1 = \boldsymbol{A}_{hk} z_1. \tag{37}$$

where, $\boldsymbol{A}_{hk} = \begin{bmatrix} 0 & 1 \\ -h_2 - k_1 & -h_1 - k_2 \end{bmatrix}$.

Thus, if the control gain matrix $\boldsymbol{K}_1$ is chosen such that $\boldsymbol{A}_{hk}$ is Hurwitz, then z_1 will exponentially converge to zeros. Therefore, the control law can be summarized as follows.

$$\begin{cases} x_{1d} = y_{1d} \\ x_{2d} = \dot{y}_{1d} \\ u_{hd} = (h_1 \dot{y}_{1d} + h_2 y_{1d} - f + \dot{x}_{2d}) \big/ h_3 \\ z_1 = x_{1d} - x_1 \\ z_2 = x_{2d} - x_2 \\ u_h = u_{hd} + \frac{1}{h_3} \boldsymbol{K}_1 z_1 \end{cases} \tag{38}$$

This controller proposed is compared with the following BC:

$$\begin{cases} z_1 = x_{1d} - x_{1r} \\ z_2 = x_{2d} - \alpha_1 \\ \alpha_1 = k_1 z_1 + \dot{x}_{1r} \\ u_h = \frac{1}{h_3}(h_1 x_2 + h_2 x_1 - f + \dot{\alpha}_1 - k_2 z_2 + z_1) \end{cases} \tag{39}$$

Remark 1: Through algebraic operations, we obtain the FBC control law for the hoisting system. From the progress of the FBC design, we can obtain that the FBC simplifies the controller design compared with the BC.

C. FBC FOR THE EHSS

Likewise, for the subsystem (25), the output is $y_2 = x_3$ and the control input is $u_L = Q_L$. Therefore, for the EHSS (25), we can obtain flatness functions from $y_2, \dot{y}_2, \ddot{y}_2$ to $\boldsymbol{x}_2$ and the control input u_L as

$$\begin{bmatrix} x_3 \\ x_4 \\ x_5 \\ u_L \end{bmatrix} = \begin{bmatrix} y_2 \\ \dot{y}_2 \\ \frac{1}{a_1}(\ddot{y}_2 + a_2 \dot{y}_2 + a_3 F_g) \\ \frac{1}{a_6}(a_4 \dot{y}_2 + a_5 x_5 + \dot{x}_5) \end{bmatrix}. \tag{40}$$

Let the desired state $\boldsymbol{x}_{2d} = [x_{3d}, x_{4d}, x_{5d}]^T = \left[y_{2d}, \dot{y}_{2d}, \frac{1}{a_1}(\ddot{y}_{2d} + a_2 \dot{y}_{2d} + a_3 F_g)\right]^T$, where y_{2d} denotes the desired output, namely, the reference signal. Therefore, the dynamics of the desired state $\boldsymbol{x}_{2d} = [x_{3d}, x_{4d}, x_{5d}]^T$ yields

$$\frac{d}{dt} \begin{bmatrix} x_{3d} \\ x_{4d} \\ x_{5d} \end{bmatrix} = \begin{bmatrix} x_{4d} \\ a_1 x_{5d} - a_2 x_{4d} - a_3 F_g \\ -a_4 x_{4d} - a_5 x_{5d} + a_6 u_L \end{bmatrix}. \tag{41}$$

Therefore, we can obtain the open-loop control input u_{Ld} as

$$u_{Ld} = \frac{1}{a_6}(a_4 \dot{y}_{2d} + a_5 x_{5d} + \dot{x}_{5d}). \tag{42}$$

Define the tracking error vector $z_2 = [z_3, z_4, z_5]^T = [x_{3d} - x_3, x_{4d} - x_4, x_{5d} - x_5]^T$. Therefore, the tracking error dynamics yields

$$\begin{bmatrix} \dot{z}_3 \\ \dot{z}_4 \\ \dot{z}_5 \end{bmatrix} = \begin{bmatrix} z_4 \\ a_1 z_5 - a_2 z_4 \\ -a_4 z_4 - a_5 z_5 + a_6 (u_{Ld} - u_L) \end{bmatrix}. \tag{43}$$

With $u_{Ld} = u_L$, we can obtain

$$\begin{bmatrix} \dot{z}_3 \\ \dot{z}_4 \\ \dot{z}_5 \end{bmatrix} = \begin{bmatrix} z_4 \\ a_1 z_5 - a_2 z_4 \\ -a_4 z_4 - a_5 z_5 \end{bmatrix}. \tag{44}$$

In matrix form,

$$\dot{z}_2 = \boldsymbol{A}_L z_2. \tag{45}$$

where, $\boldsymbol{A}_L = \begin{bmatrix} 0 & 1 & 0 \\ 0 & -a_2 & a_1 \\ 0 & -a_4 & -a_5 \end{bmatrix}$.

We design the control input with state feedbacks as

$$u_L = u_{Ld} + \frac{1}{a_6} \boldsymbol{K}_2 z_2. \tag{46}$$

where $\boldsymbol{K}_2 = [k_3, k_4, k_5]^T$. The tracking error dynamics with state feedbacks yields

$$\dot{z}_2 = \boldsymbol{A}_{Lk} z_2. \tag{47}$$

where, $\boldsymbol{A}_{Lk} = \begin{bmatrix} 0 & 1 & 0 \\ 0 & -a_2 & a_1 \\ -k_3 & -a_4 - k_4 & -a_5 - k_5 \end{bmatrix}$.

Thus, if the control gain matrix $\boldsymbol{K}_2$ is chosen such that $\boldsymbol{A}_{Lk}$ is Hurwitz, then z_2 will exponentially converge to zeros. Therefore, the control law can be summarized as follow.

$$\begin{cases} x_{3d} = y_{2d} \\ x_{4d} = \dot{y}_{2d} \\ x_{5d} = \frac{1}{a_6}(\ddot{y}_{2d} + a_4 \dot{y}_{2d} + a_5 y_{2d} - a_3 F_g) \\ u_{Ld} = \frac{1}{a_6}(a_4 x_{4d} + a_5 x_{5d} + \dot{x}_{5d}) \\ z_3 = x_{3d} - x_3 \\ z_4 = x_{4d} - x_4 \\ z_5 = x_{5d} - x_5 \\ u_L = u_{Ld} + \frac{1}{a_6} \boldsymbol{K}_2 z_2. \end{cases} \tag{48}$$

This controller proposed is compared with the following BC:

$$\begin{cases} z_3 = x_{3d} - x_3 \\ z_4 = \alpha_3 - x_4 \\ z_5 = \alpha_4 - x_5 \\ \alpha_3 = -k_3 z_3 + \dot{x}_{3d} \\ \alpha_4 = \frac{1}{a_1}\left(z_3 + a_2 x_4 - \frac{F_g}{a_3} + \dot{\alpha}_3 + k_4 z_4\right) \\ u_L = \frac{1}{a_6}(k_5 z_5 + \dot{\alpha}_4 + a_4 x_4 + a_5 x_5 + a_1 z_4). \end{cases} \tag{49}$$

Remark 2: Through a series of algebraic operations, we obtain the FBC control law of the hydraulic subsystem. From the progress of the FBC design, we can obtain: 1) The FBC simplify the controller design than the BC.

FIGURE 5. The experiment setup of the DRWHS.

Time derivatives of virtual controls α_3 and α_4, especially, the time derivative of the virtual control α_4, will definitely increase the compute and the complex of the BC's design largely; 2) The FBC will not need time derivatives of system states, which will not amplify measurement noises and unmodeled characteristics.

D. STABILITY OF THE CLOSED-LOOP

In order to prove the stability of the closed loop, we have the following proposition.

Proposition: With error derivatives and, if positive definite matrices $\boldsymbol{P}_h, \boldsymbol{P}_L$, and control gains $\boldsymbol{K}_1, \boldsymbol{K}_2$ are properly chosen, such that $\boldsymbol{P}_h\boldsymbol{A}_{hk} + \boldsymbol{A}_{hk}^T\boldsymbol{P}_h \leq 0$ and $\boldsymbol{P}_h\boldsymbol{A}_{Lk} + \boldsymbol{A}_{Lk}^T\boldsymbol{P}_h \leq 0$, then the stability of the closed loop can be guaranteed by the proposed control law.

Proof: We define a Lyapunov candidate function V as

$$V = z_1^T\boldsymbol{P}_h z_1 + z_2^T\boldsymbol{P}_L z_2. \tag{50}$$

The derivative of Eq. (48) with time yields

$$\dot{V} = z_1^T\left(\boldsymbol{P}_h\boldsymbol{A}_{hk} + \boldsymbol{A}_{hk}^T\boldsymbol{P}_h\right)z_1 + z_2^T\left(\boldsymbol{P}_h\boldsymbol{A}_{Lk} + \boldsymbol{A}_{Lk}^T\boldsymbol{P}_h\right)z_2 \leq 0. \tag{51}$$

Therefore, the closed-loop of the DRWHS control system is asymptotic stability.

IV. EXPERIMENTAL STUDIES

A. EXPERIMENTAL SETUP

FIGURE 5 presents the experiment setup of the DRWHS. Main structural parameters of the experiment setup are shown in TABLE 1.

TABLE 1. Structural parameters of the experiment setup.

Structural parameters	Values
Height of the experiment setup / m	7
Length of the flexible guide / m	6
Width of the experiment setup / m	3.4
Length of the experiment setup / m	4.4
Diameter of movable headgear sheaves / m	0.4
Weight of the conveyance / kg	200
Size of the weight stacks / m	0.375*0.375*0.125
Maximum acceleration / m/s^2	1
Maximum hoisting velocity / m/s	1

From FIGURE 5, in order to make the hoisting system stable, the main mechanical body of the hoisting system is welded on the ground in a frame mode. Two hydraulic winches, which have two built-in reducers, two balance valves and two brake devices, are installed on both sides of the mechanical frame with symmetrical distributions. Two hydraulic winches are fixed on the foundation by foot bolts, and two rotary encoders are connected with output shafts of two hydraulic winches respectively. Two proportional valves are utilized to control two hydraulic winches, which will form a closed-loop with two rotary encoders. Two wire ropes are connected with the conveyance through two hydraulic winches and two headgear sheaves. Two force sensors are connected between the conveyance and two wire ropes. Two hydraulic cylinders with 70 mm bore and 50 mm rod are fixed between two movable headgear sheaves and the foundation with supports welding on the foundation. Two displacement sensors are installed on the same side of two hydraulic cylinders. Sliding bars of two displacement sensors and piston rods of the hydraulic cylinder are fixed together through

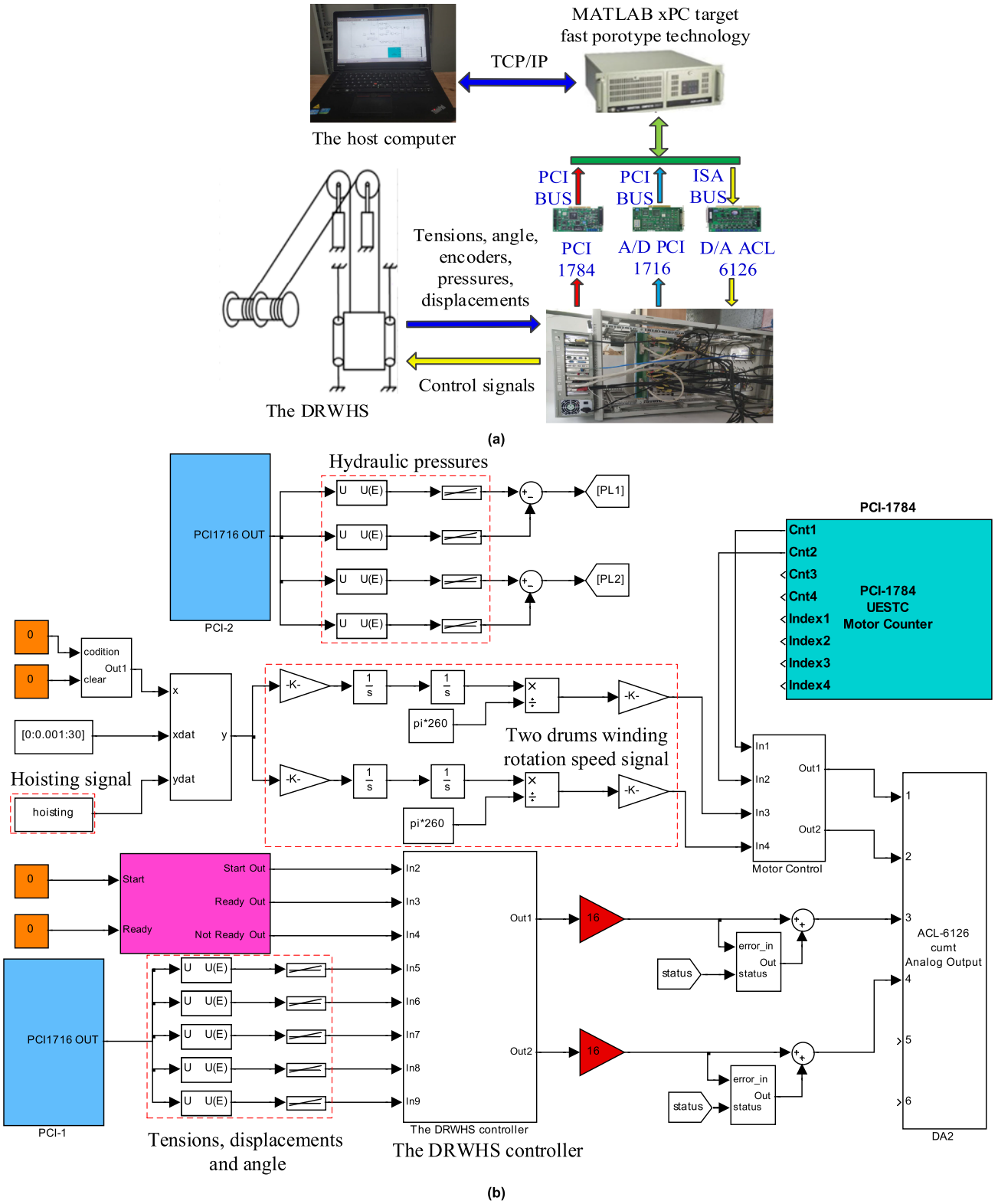

FIGURE 6. The control system. (a) The schematic diagram of the control system. (b) The main program of the control system.

two universal joints, which indicates that when hydraulic cylinders actively drive movable headgear sheaves to adjust tensions of two wire ropes, displacement sensors will measure displacements in real time.

FIGURE 6 shows the schematic diagram of the control system, which is established based on MATLAB xPC target fast prototyping technology. Hardware of the control system mainly consists of a host computer, a target computer

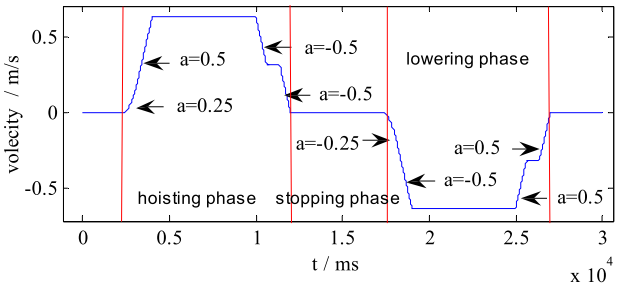

FIGURE 7. Velocity for hoisting and lowering the conveyance.

TABLE 2. Parameters of the DRWHS.

Parameters	Values	Parameters	Values
A_p	1.88×10^{-3} m^2	m_c	200 kg
b_1	0.0625 m	b_2	0.0625 m
a_2	0.1575 m	V_t	0.96×10^{-3} m^3
ΔP_r	6×10^6 Pa	$u_{\max}$	10 V
K_c	2×10^{-12} m^3/s/Pa	P_s	15×10^6 Pa
K_{sv}	4 m^3/s/A	Q_r	38 L/min
l_{120}, l_{220}	6 m	β_e	6.9×10^8 Pa
B_p	25000 N(m/s)	n_H	2
a_1	0.1575 m	n_R	4
C_{tl}	9.2×10^{-17} m^3/s/Pa	I_c	3.307 kg·m^2
ρ	0.417 kg/m		

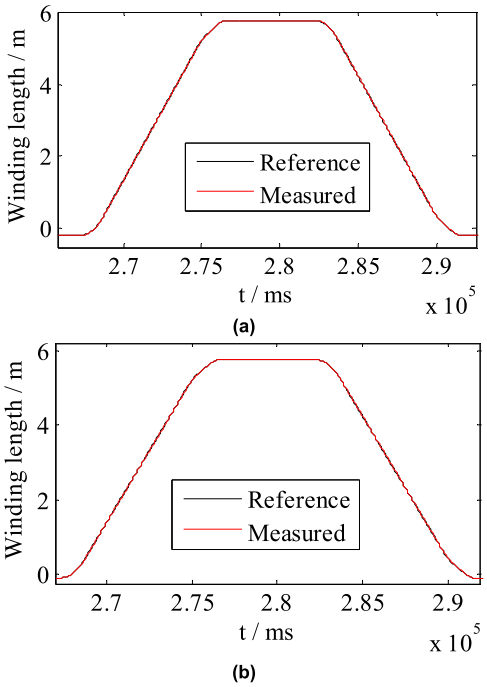

FIGURE 8. Winding length tracking performance of two Hydraulic winches. (a) Hydraulic winch 1. (b) Hydraulic winch 2.

ADVANTECH IPC-610, a signal conditioning system, two A/D board PCI-1716s, a D/A board ACL-6126, a pulse board PCI-1784 and some auxiliary accessories. The board PCI-1784, two board PCI-1716s and the board ACL-6126 are all installed in the target computer. Analog control signals from the board ACL-6126 and optimized by the signal conditioning system, are sent to servo valves for control of two hydraulic cylinders and two hydraulic winches. Analog signals from displacements of two hydraulic cylinders, tensions of two wire ropes, angle of the conveyance, and pressures of four hydraulic cylinder chambers, which will be optimized by the signal conditioning system, are transformed into digital signals by two boards PCI-1716, and impulse signals from rotation speeds of the two hydraulic winches are transformed into digital signals by the board PCI-1784. Control strategies, which are programmed by MATLAB/Simulink on the host computer, are compiled to C codes by the Microsoft Visual Studio software before they are downloaded into the target computer for real time execution. The host and target computers are communicated by Ethernet. The sampling time of the control system is 1 ms.

FIGURE 7 presents the six-stage velocity planning scheme for the DRWHS. a denotes the acceleration in the hoisting phase or the lowering phase, and the unit is m/s^2.

B. EXPERIMENTAL RESULTS

TABLE 2 shows key parameters of the DRWHS in experiments.

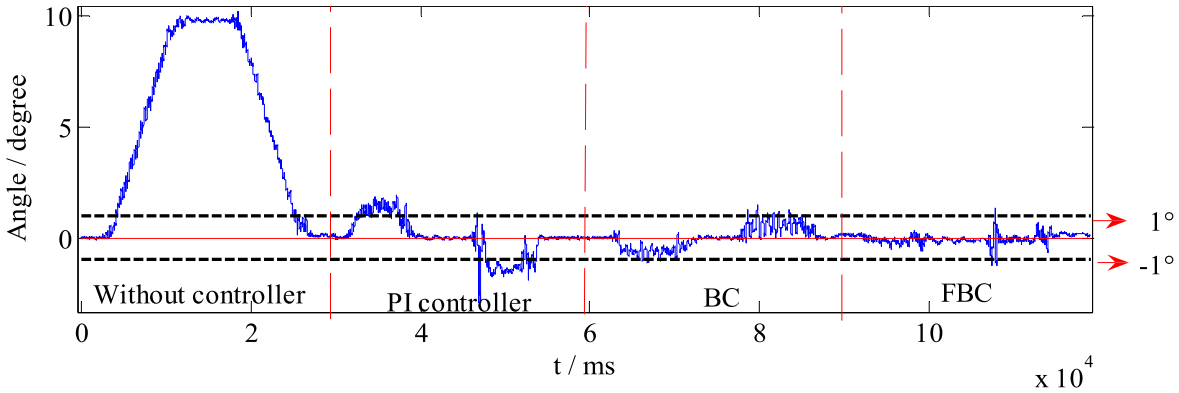

FIGURE 9. The counterclockwise rotation angle in hoisting and lowering the conveyance: 1) without any a controller; 2) with the PI controller; 3) with the BC; 4) with the FBC.

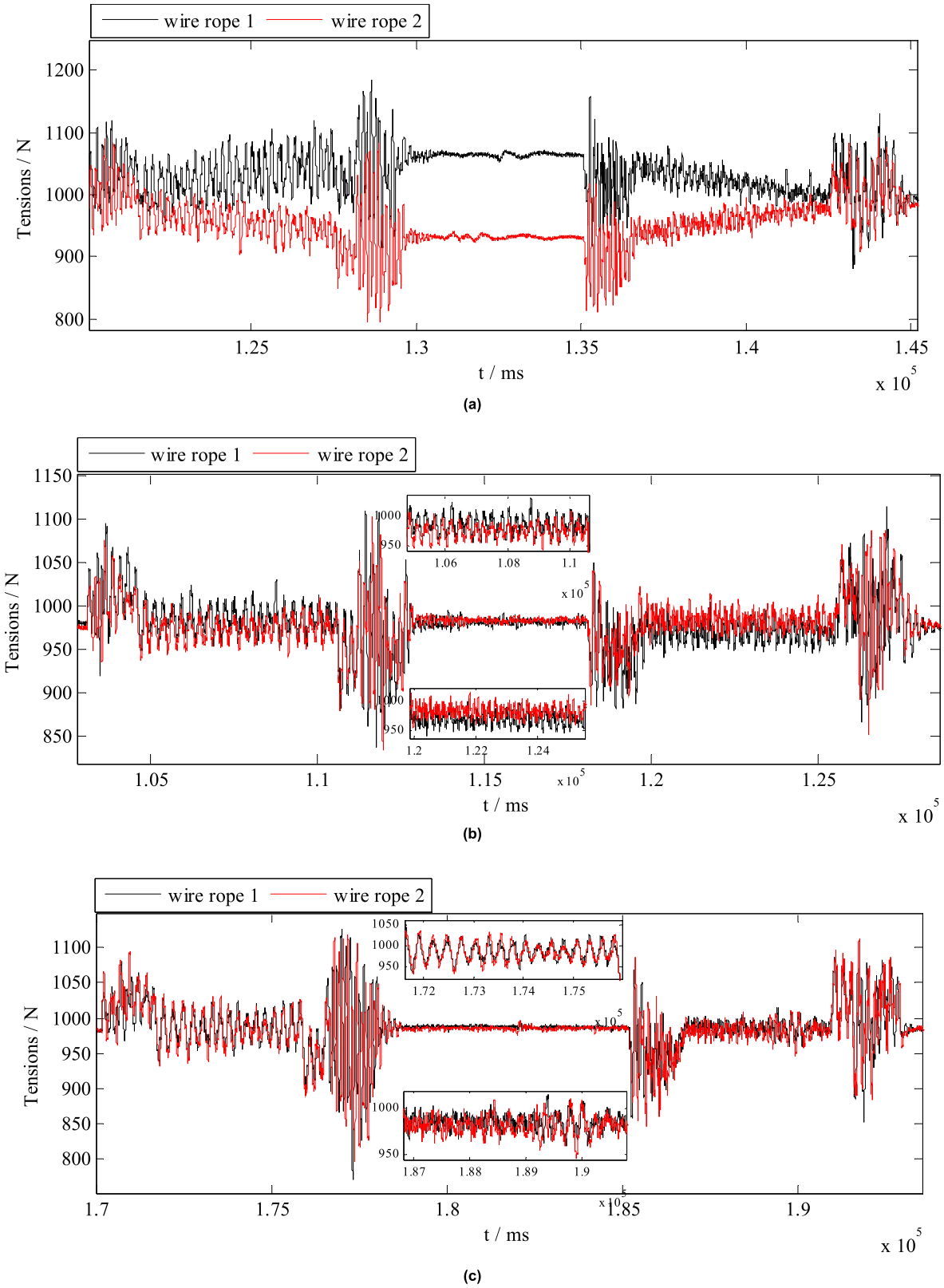

FIGURE 10. Tensions of two wire ropes and the tension difference in hoisting and lowering the conveyance: 1) without any a controller; 2) with the PI controller; 3) with the BC; 4) with the FBC. (a) Without any a controller. (b) With the PI controller. (c) With the BC. (d) With the FBC. (e) The tension difference.

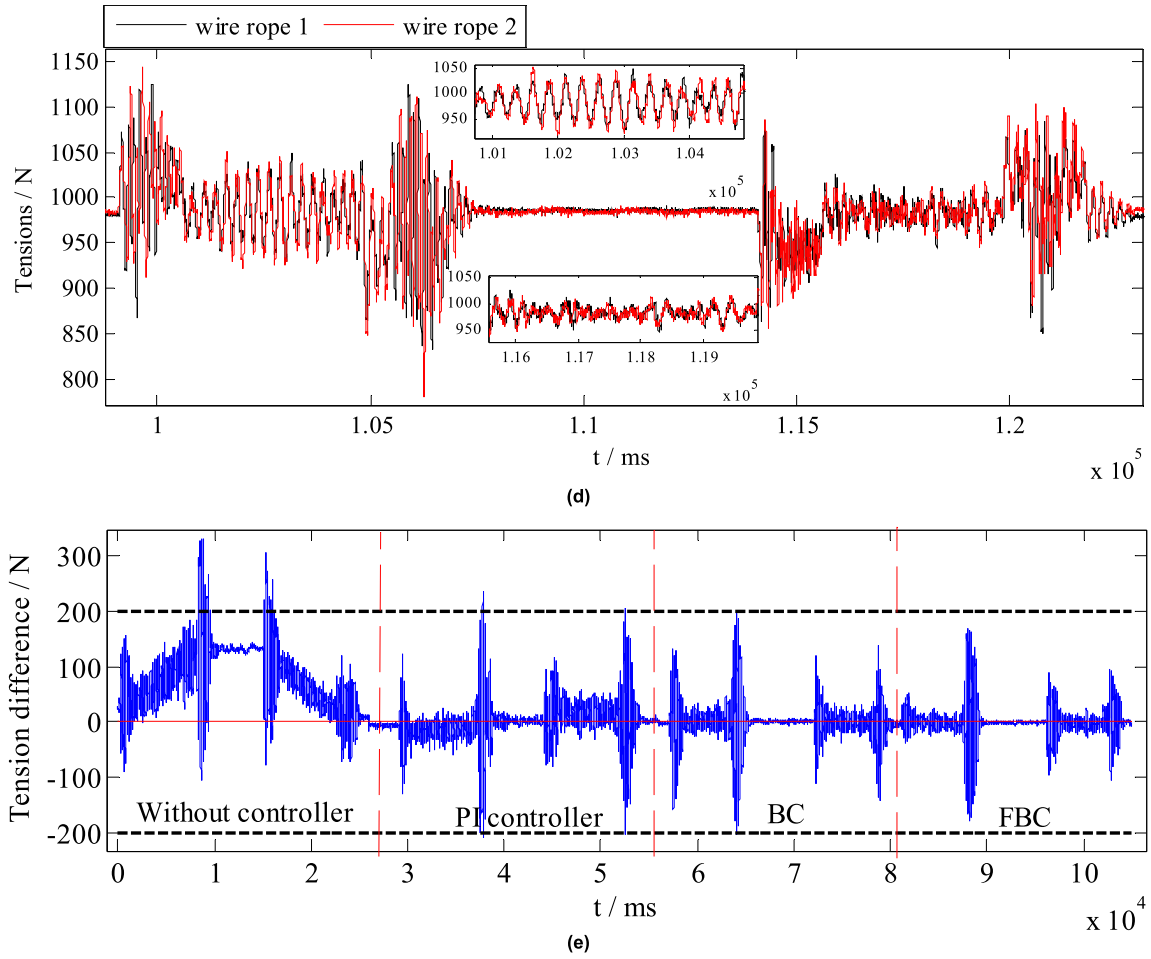

FIGURE 10. ***(Continued.)*** **Tensions of two wire ropes and the tension difference in hoisting and lowering the conveyance: 1) without any a controller; 2) with the PI controller; 3) with the BC; 4) with the FBC. (a) Without any a controller. (b) With the PI controller. (c) With the BC. (d) With the FBC. (e) The tension difference.**

In order to verify the performance of three control strategies, a series of experimental tests were conducted on the DRWHS. The desired counterclockwise rotation angle of the conveyance is undoubtedly 0 degree. FIGURE 8 presents the reference winding lengths of two hydraulic winches and their real-time measurement signals. From FIGURE 8, two hydraulic winches can track reference winding lengths accurately. FIGURE 9 and 10 shows comparison results with three different control strategies. Comparison between three different control strategies is explicitly stated as follows. Control gains of the three controller are presented in Table 3.

1) PI controller: Control inputs u_1 and u_2, which are designed by the counterclockwise rotation angle θ, is expressed as $u = K_p\theta + K_I \sum \theta = u_1 = \text{-}u_2$.
2) BC: Control inputs are obtained by the BC based on the nonlinear dynamic model of the DRWHS.
3) FBC: In this controller, control inputs are obtained by the FBC, which is insensitive to the unmodeled characteristics of the DRWHS and measurement noises of sensors.

TABLE 3. **Control gains of the three controllers.**

The PI controller			
In the hoisting system		In the EHSS	
K_p	0.15	K_{hp}	17
K_I	0.5	K_{hI}	0
The BC			
In the hoisting system		In the EHSS	
k_1	0.017	k_3	1400
k_2	0.022	k_4	950
		k_5	950
The FBC			
In the hoisting system		In the EHSS	
k_1	1.6×10^7	k_3	2.9×10^{12}
k_2	3×10^5	k_4	1×10^9
		k_5	10

FIGURE 9 gives the counterclockwise rotation angle in hoisting and lowering the conveyance: 1) without any a controller; 2) with the PI controller; 3) with the BC; 4) with the FBC. As shown in FIGURE 8, without any a controller, the counterclockwise rotation angle of the conveyance

TABLE 4. RMSE of three controllers.

Controllers	Peak error	RMSE
The counterclockwise rotation angle		
The PI controller	2.96°	0.8551
The BC	1.48°	0.473
The FBC	1.14°	0.1703
The tension difference		
The PI controller	236.45 N	35.0227
The BC	203.99 N	32.5742
The FBC	179.11 N	28.3574

gradually increases at the hoisting stage, then stays at a certain value (approximate 10°) at the stop stage, and then gradually decreases to zero at the lowering stage. When the PI controller, the BC and the FBC are employed, the change of the counterclockwise rotation angle is effectively controlled and the counterclockwise rotation angle reaches 2.96°, 1.48° and 1.14°. And changes of the counterclockwise rotation angle of the FBC is steadier than the BC and the PI controller. In conclusion, it is obviously that performances of three controllers can be stated as follows: the FBC > the BC > the PI controller.

FIGURE 10 shows tensions of two wire ropes and the tension difference in hoisting and lowering the conveyance: 1) without any a controller; 2) with the PI controller; 3) with the BC; 4) with the FBC. From FIGURE 10 (a) and (e), without any a controller, the tension difference increase gradually with fluctuations, then stays approximately at a certain value with fluctuations, and then decrease to zero with fluctuations. From FIGURE 10 (b), when the PI controller is employed to actively coordinate the tension difference of two wire ropes, the tension difference decrease efficiently. From the local enlarged figure in FIGURE 10 (b), changes of tensions of two wire ropes are consistent but there is still a certain tension difference between two wire ropes. And the performance of the PI controller need to be improved. From FIGURE 10 (c), when the BC are utilized, tensions of two wire ropes are consistent in the hoisting stage but not consistent in the lowering stage. From FIGURE 10 (d), when the FBC are utilized, tensions of two wire ropes are consistent in the hoisting and the lowering stage. From FIGURE 10 (e), tension differences of three controllers reach 236.45 N, 203.99 N and 179.11 N respectively. In summary, performances of three controllers: the FBC > the BC > the PI controller.

In order to further illustrate the performance of three controllers, the root mean square error (RMSE) is employed, which can be expressed as

$$\mathrm{RMSE} = \sqrt{\frac{\sum_{i}^{n} \left(R_{in,i} - R_{out,i}\right)^2}{n}} \tag{52}$$

where $R_{in,i}$ denotes the reference signal, $R_{out,i}$ denotes the feedback signal from sensors, n denotes the length of the signal. The results of the RMSE is presented in TABLE 4.

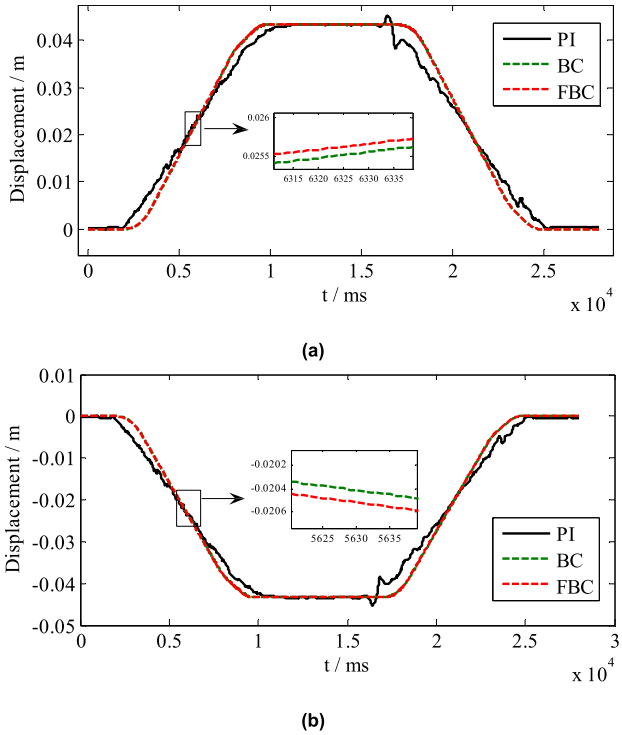

FIGURE 11. Displacements of two hydraulic cylinders with three different controllers: the PI controller, the BC, and the FBC. (a) Hydraulic cylinder 1. (b) Hydraulic cylinder 2.

From TABLE 4, it is can be seen that the FBC exhibits a better performance than the BC and the PI controller.

FIGURE 11 presents displacements of two hydraulic cylinders in hoisting and lowering the conveyance. From FIGURE 10, change ranges of two hydraulic cylinders of the PI controller are large but those of the BC and FBC are relatively steadier. From the local enlarge figure in FIGURE 10, it can be seen that the FBC is faster than the BC when actively adjusting tensions of two wire ropes, which indicates that the performance of the FBC is better than that of the BC. Therefore, the FBC exhibits better performance than the BC and the PI controller.

V. CONCLUSION

The DRWHS is a typical complex machine-electricity-hydraulic system, which indicates that its accurate dynamic model is usually hard to obtain. In order to improve the coordination of tensions of two wire ropes of the DRWHS, a FBC, which is insensitive to measurement noises of sensors and unmodeled characteristics, is employed to actively coordinate tensions of two wire ropes. Experimental results show that the proposed controller exhibits a better performance than the BC and the conventional PI controller. Therefore, the full text can be summarized as follows.

(1) The nonlinear model of the hoisting system is expressed with a state space representation. The nonlinear model of the EHSS is established and is expressed

with a state space representation. Therefore, the state space representation of the DRWHS is shown.

(2) Through a series of algebraic operations, system states and system inputs of the hoisting system and the EHSS are expressed with system outputs and a finite number of their time derivatives. And then, the control law of the proposed controller is shown. Compared with the BC, the proposed controller has prominent advantages: 1) lower controller design complication; 2) no need for repeated derivation of virtual control in the controller' design so that measurement noises of sensors and unmodeled characteristics will not be amplified, which will further improve the coordination of tensions of two wire ropes.

(3) The experimental bench is elaborately introduced to verify the performance of the proposed controller. Experimental results show that the proposed controller made the conveyance steadier than the BC and the PI controller: 1) the tracking error of the counterclockwise rotation angle of the conveyance is smaller than the BC and the PI controller; 2) the tension difference is smaller than the BC and the PI controller.

REFERENCES

[1] X. Li, Z.-C. Zhu, and G. Shen, "A switching-type controller for wire rope tension coordination of electro-hydraulic-controlled double-rope winding hoisting systems," *Proc. Inst. Mech. Eng. I, J. Syst. Control Eng.*, vol. 230, no. 10, pp. 1126–1144, Nov. 2016.

[2] S. Kaczmarczyk and W. Ostachowicz, "Transient vibration phenomena in deep mine hoisting cables. Part 1: Mathematical model," *J. Sound Vib.*, vol. 262, no. 2, pp. 219–244, 2003.

[3] S. Kaczmarczyk and W. Ostachowicz, "Transient vibration phenomena in deep mine hoisting cables. Part 2: Numerical simulation of the dynamic response," *J. Sound Vib.*, vol. 262, no. 2, pp. 245–289, Apr. 2003.

[4] A. Carbogno, "Mine hoisting in deep shafts in the 1st half of 21st century," *Acta Montanistica Slovaca*, vol. 7, no. 3, pp. 188–192, Aug. 2002.

[5] J. Yao, X. Xiao, A. Peng, Y. Jiang, and C. Ma, "Assessment of safety for axial fluctuations of head sheaves in mine hoist based on coupled dynamic model," *Eng. Failure Anal.*, vol. 51, pp. 98–107, May 2015.

[6] B. M. Brentan, E. Luvizotto, Jr., I. Montalvo, J. Izquierdo, and R. Pérez-García, "Position control of nonlinear hydraulic system using an improved PSO based PID controller," *Procedia Eng.*, vol. 83, pp. 241–259, 2017.

[7] S. Srivastava and V. S. Pandit, "A PI/PID controller for time delay systems with desired closed loop time response and guaranteed gain and phase margins," *J. Process Control*, vol. 37, pp. 70–77, Jan. 2016.

[8] J. Liu, S. Vazquez, L. Wu, A. Marque, H. Gao, and L. G. Franquelo, "Extended state observer-based sliding-mode control for three-phase power converters," *IEEE Trans. Ind. Electron.*, vol. 64, no. 1, pp. 22–31, Jan. 2017.

[9] F. Li, L. Wu, P. Shi, and C.-C. Lim, "State estimation and sliding mode control for semi-Markovian jump systems with mismatched uncertainties," *Automatica*, vol. 51, pp. 385–393, Jan. 2015.

[10] M. Chen, P. Shi, and C. C. Lim, "Robust constrained control for MIMO nonlinear systems based on disturbance observer," *IEEE Trans. Autom. Control*, vol. 60, no. 12, pp. 3281–3286, Dec. 2015.

[11] B. P. G. Van Parys, D. Kuhn, P. J. Goulart, and M. Morari, "Distributionally robust control of constrained stochastic systems," *IEEE Trans. Autom. Control*, vol. 61, no. 2, pp. 430–442, Feb. 2016.

[12] X. H. Chang, C. Yang, and J. Xiong. "Quantized fuzzy output feedback H_∞ control for nonlinear systems with adjustment of dynamic parameters," *IEEE Trans. Syst., Man, Cybern. Syst.*, vol. 49, no. 10, pp. 2005–2015, Oct. 2019. doi: 10.1109/TSMC.2018.2867213.

[13] L. Ma, X. Huo, X. Zhao, B. Niu, and G. Zong, "Adaptive neural control for switched nonlinear systems with unknown backlash-like hysteresis and output dead-zone," *Neurocomputing*, vol. 357, pp. 203–214, Sep. 2019.

[14] H. Wang, P. X. Liu, J. Bao, X. J. Xie, and S. Li, "Adaptive neural output-feedback decentralized control for large-scale nonlinear systems with stochastic disturbances," *IEEE Trans. Neural Netw. Learn. Syst.*, to be published. doi: 10.1109/TNNLS.2019.2912082.

[15] X. Huo, L. Ma, X. Zhao, B. Niu, and G. Zong, "Observer-based adaptive fuzzy tracking control of MIMO switched nonlinear systems preceded by unknown backlash-like hysteresis," *Inf. Sci.*, vol. 490, pp. 369–386, Jul. 2019.

[16] H. Wang, P. X. Liu, X. Zhao, and X. Liu, "Adaptive fuzzy finite-time control of nonlinear systems with actuator faults," *IEEE Trans. Cybern.*, to be published. doi: 10.1109/TCYB.2019.2902868.

[17] Z.-C. Zhu, X. Li, G. Shen, and W.-D. Zhu, "Wire rope tension control of hoisting systems using a robust nonlinear adaptive backstepping control scheme," *ISA Trans.*, vol. 72, pp. 256–272, Jan. 2018.

[18] J. Yao, Z. Jiao, and D. Ma, "Extended-state-observer-based output feedback nonlinear robust control of hydraulic systems with backstepping," *IEEE Trans. Ind. Electron.*, vol. 61, no. 11, pp. 6285–6293, Nov. 2014.

[19] G. Ma, C. Chen, Y. Lyu, and Y. Guo, "Adaptive backstepping-based neural network control for hypersonic reentry vehicle with input constraints," *IEEE Access*, vol. 6, pp. 1954–1966, 2017.

[20] X. Yu and Y. Lin, "Adaptive backstepping quantized control for a class of nonlinear systems," *IEEE Trans. Autom. Control*, vol. 62, no. 2, pp. 981–985, Feb. 2017.

[21] Z. Zheng and Y. Zou, "Adaptive integral LOS path following for an unmanned airship with uncertainties based on robust RBFNN backstepping," *ISA Trans.*, vol. 65, p. 210–219, Nov. 2016.

[22] Q. Guo, Y. Zhang, B. Celler, and S. Su, "Backstepping control of electro-hydraulic system based on extended-state-observer with plant dynamics largely unknown," *IEEE Trans. Ind. Electron.*, vol. 63, no. 11, pp. 6909–6920, 2016.

[23] J. A. Farrell, M. Polycarpou, M. Sharma, and W. Dong, "Command filtered backstepping," *IEEE Trans. Autom. Control*, vol. 54, no. 6, pp. 1391–1395, Jun. 2009.

[24] W. Dong, J. A. Farrell, M. M. Polycarpou, V. Djapic, and M. Sharma, "Command filtered adaptive backstepping," *IEEE Trans. Control Syst. Technol.*, vol. 20, no. 3, pp. 566–580, May 2012.

[25] Y. Pan, H. Wang, X. Li, and H. Yu, "Adaptive command-filtered backstepping control of robot arms with compliant actuators," *IEEE Trans. Control Syst. Technol.*, vol. 26, no. 3, pp. 1149–1156, Mar. 2018.

[26] M. Fliess, J. Lévine, P. Martin, and P. Rouchon, "Flatness and defect of non-linear systems: Introductory theory and examples," *Int. J. Control*, vol. 61, no. 6, pp. 1327–1361, 1995.

[27] T. J. Koo and S. Sastry, "Differential flatness based full authority helicopter control design," in *Proc. 38th IEEE Conf. Decis. Control*, Phoenix, AZ, USA, Dec. 1999, pp. 1982–1987.

[28] H. Sira-Ramirez and C. A. Ibanez, "The control of the hovercraft system: A flatness based approach," in *Proc. IEEE Int. Conf. Control Appl.*, Anchorage, AK, USA, Sep. 2000, pp. 692–697.

[29] R. Mahadevan, S. K. Agrawal, and F. J. Doyle, "Differential flatness based nonlinear predictive control of fed-batch bioreactors," *Control Eng. Pract.*, vol. 9, no. 8, pp. 889–899, Aug. 2001.

[30] A. Houari, H. Renaudineau, J.-P. Martin, S. Pierfederici, and F. Meibody-Tabar, "Flatness-based control of three-phase inverter with output *LC* filter," *IEEE Trans. Ind. Electron.*, vol. 59, no. 7, pp. 2890–2897, Jul. 2012.

[31] J. M. Rodriguez-Fortun, J. Orus, J. Alfonso, F. B. Gimeno, and J. A. Castellanos, "Flatness-based active vibration control for piezoelectric actuators," *IEEE/ASME Trans. Mechatronics*, vol. 18, no. 1, pp. 221–229, Feb. 2013.

[32] J. M. Rodriguez-Fortun, J. Orus, J. Alfonso, J. R. Sierra, F. Buil, F. Rotella, and J. A. Castellanos, "Model-based mechanical and control design of a three-axis platform," *Mechatronics*, vol. 22, no. 7, pp. 958–969, Oct. 2012.

[33] R. Bindel, R. Nitsche, R. Rothfuß, and M. Zeitz, "Flatness based control of a two valve hydraulic joint actuator of a large manipulator," in *Proc. Eur. Control Conf. (ECC)*, Karlsruhe, Germany, Aug./Sep. 1999, pp. 3190–3195.

[34] T. Wey, M. Lemmen, and W. Bernzen, "Hydraulic actuators for flexible robots: A flatness based approach for tracking and vibration control," in *Proc. Eur. Control Conf. (ECC)*, Karlsruhe, Germany, Aug./Sep. 1999, pp. 2949–2954.

[35] W. Kim, D. Won, and M. Tomizuka, "Flatness-based nonlinear control for position tracking of electrohydraulic systems," *IEEE/ASME Trans. Mechatronics*, vol. 20, no. 1, pp. 197–206, Feb. 2015.

[36] D. Zheng and H. Xu, "Adaptive backstepping-flatness control based on an adaptive state observer for a torque tracking electrohydraulic system," *IEEE/ASME Trans. Mechatronics*, vol. 21, no. 5, pp. 2440–2452, Oct. 2016.
[37] C. Jing, H. Xu, and J. Jiang, "Flatness-based adaptive nonlinear control for torque tracking of electro-hydraulic friction load simulator with uncertainties," *Proc. Inst. Mech. Eng. I, J. Syst. Control Eng.*, vol. 233, no. 8, pp. 1009–1016, Sep. 2019. doi: 10.1177/0959651818813230.
[38] C. Jing, H. Xu, X. Song, and B. Lu, "Adaptive extended state observer-based flatness nonlinear output control for torque tracking of electro-hydraulic loading system," *Trans. Inst. Meas. Control*, vol. 40, no. 10, pp. 2999–3009, Jun. 2018.
[39] H. Du, Q. Zhang, S. Chen, and J. Fang, "Modeling, simulation, and experimental validation of electro-hydraulic power steering system in multi-axle vehicles," *Proc. Inst. Mech. Eng., D, J. Automobile Eng.*, vol. 233, no. 2, pp. 317–332, Feb. 2019.
[40] G. J. Krige, "Guidelines for the design of rope guides," in *Proc. Int. Conf. Hoisting Haulage*, 2005, pp. 28–275.

WANSHUN ZANG received the M.S. degree from Jiamusi University, in 2016. He is currently pursuing the Ph.D. degree with the School of Mechatronic Engineering, China University of Mining and Technology. His research interests include electro-hydraulic servo control, fault-tolerant control, and wire rope tension control.

GANG SHEN received the B.S. degree from Jiamusi University, in 2005, and the M.S. and Ph.D. degrees from the Harbin Institute of Technology, in 2007 and 2011, respectively. He is currently a Professor with the School of Mechanical and Electrical Engineering, China University of Mining and Technology. His research interests include electro-hydraulic servo control, parallel robot, and loading systems.

GUANGCHAO RUI received the B.S. degree from Northern Jiaotong University, in 1999, and the M.S. degree from the Harbin Institute of Technology, in 2009. He is currently a Senior Engineer with the Seventh Thirteen Institute of China Shipbuilding Industry Corporation. His research interests include electro-hydraulic servo control and design of electrical systems.

XIANG LI received the B.S. and Ph.D. degrees from the China University of Mining and Technology, in 2013 and 2018, respectively, where he currently holds a postdoctoral position at the School of Mechanical and Electrical Engineering. His research interests include electro-hydraulic servo control, force control, and wire rope tension control of hoisting systems.

GE LI received the M.S. degree from the China University of Mining and Technology, in 2012, where she is currently pursuing the Ph.D. degree with the School of Mechatronic Engineering. Her research interests include parallel mechanism control, electro-hydraulic servo control, and vibration control.

YU TANG received the B.S. and Ph.D. degrees from the China University of Mining and Technology, in 2011 and 2016, respectively, where he is currently a Lecturer with the School of Mechanical and Electrical Engineering. His research interests include electro-hydraulic servo control, acceleration control, and force control.